MecSol2013
International Symposium on Solid Mechanics
April 18-19, 2013
Porto Alegre, Rio Grande do Sul, Brazil

EFFECTS OF LATERAL MOVEMENTS ON THE DEFORMATION OF SEDIMENTARY BASINS: A NUMERICAL APPROACH

André Brüch
Department of Civil Engineering
Federal University of Rio Grande do Sul, Porto Alegre – RS, Brazil
andrebruch@hotmail.com

Denise Bernaud
Department of Civil Engineering
Federal University of Rio Grande do Sul, Porto Alegre – RS, Brazil
bernaud@ppgec.ufrgs.br

Samir Maghous
Department of Civil Engineering
Federal University of Rio Grande do Sul, Porto Alegre – RS, Brazil
samir.maghous@ufrgs.br

ABSTRACT

The process of mechanical compaction of a sedimentary basin in fully saturated conditions takes place through water expulsion from the porous material, thus resulting in grain repacking and volume reduction. The rate of this volume reduction is primarily dependent on the amount and rate of sediment accretion and the permeability of the sediment material. In absence of tectonic-driven deformation, a deposited sedimentary layer compacts as the excess pore-pressure generated by its own weight dissipates progressively. Nevertheless, tectonic loading increases substantially the excess pore-pressure gradient, thus accelerating the compaction process. This work is devoted to the modeling of purely mechanical compaction of a sedimentary basin. Three phases are concurrently or consecutively involved in the latter process: the sediments deposition, its compaction due to gravitational forces and pore-pressure dissipation, and deformation induced by extensional and/or compressive tectonic motion. A specific computational procedure has been developed to perform numerical simulations in plane strain conditions via the finite element method. The poromechanical constitutive law is formulated in the framework of finite irreversible strains, accounting for hydromechanical and elasticity-plasticity couplings. Comparisons are made for both cases: gravitational compaction only and compaction followed by efforts of tectonic origin.

Keywords: Sedimentary basin, Finite poroplasticity, Tectonic loading.

1 INTRODUCTION

Sedimentary basins are associated with a specific region of the planet crust that was able to retain an appreciable amount of sediments originated from destruction of any type of rock. These sediments are transported and deposited in different types of environments (continental, marine or intermediate), where they are transformed into rock through natural phenomena involving physical and chemical processes.

The study of sedimentary basins is an important issue in the field of geophysics and geomechanics that seeks understanding the geological history and reconstructing the

poromechanical history of many regions of the planet. The potential applications include petroleum exploration, reserve assessment and production. They are important aquifers and a large variety of metallic and non metallic minerals can be also found in this kind of geological formation. Detection and exploration of all these resources requires sophisticated prediction tools and technical methods, which have been developed in many ways along the past decades. Much of this evolution is due to the oil industry, where a need for knowledge on the subject of oil reservoirs has led to enormous expansion of research on modern sedimentary environments. Today it is possible to make quite detailed predictions for the origin of hydrocarbon and water reservoirs from a combination of three-dimensional seismic reflection profiles, electric log signatures and downhole probes [1].

However, the progress in this field has been hampered by the absence of good models to describe the rheological behavior of the constituent material of the problem. Since it is a multidisciplinary problem, the numerical simulation of all the coupling phenomena that are controlling the basin deformation proves very difficult, leading some authors to give priority to only certain components in the formulation of their models.

In the context of deep oceanic basins, the processes that affect the compaction of sediments can be divided into two main groups: mechanical and chemical. Mechanical compaction is mainly because of the excess pore-pressure dissipation and deformation imposed by tectonics. A load suddenly applied is at first carried by the pore water (as excess pore-water pressure) and gradually transferred to the sediment structure. The compaction results from the decrease of pore space through grain repacking and the expulsion of water. The speed of this volume reduction is primarily dependent on the amount and rate of load application and the permeability of the sediment. The mechanical compaction is completed when the excess pore-water pressure is zero and pore-water pressure is solely hydrostatic [2]. Chemical compaction involves dissolution-precipitation mechanisms, generally induced by stress (intergranular pressure-solution). Nevertheless, it is important to note that these are interdependent processes, although mechanical phenomena prevail in the upper layers of sedimentary basins, whereas chemical compaction is dominant in the deeper layers, where stresses and temperatures are higher [3].

The basic models of mechanical compaction are still based on phenomenological relationships relating porosity to effective vertical stress. The concept of porosity versus Terzaghi's effective stress dependence has been early introduced by Hubbert and Rubey [4] and later by Smith [5]. These ideas have been widely adopted and implemented in numerical finite element models that have yielded valuable contributions to the understanding of the evolution of sedimentary basins. Interestingly noting, Gibson [6] can be considered one of the pioneer works that introduced consolidation theory for analyzing sediment compaction. The fundamental assumptions of the latter work were: constant sedimentation rate, a single lithology, constant sediment properties and Therzaghi's small strain consolidation theory. The approach was mainly applied to the analysis of consolidation in shallow soil deposits.

On the other hand, the lateral movements induced by tectonic events influence strongly the formation of sedimentary basins. The rate and manner as the tectonic plates move relatively to each other govern many aspects of the geodynamic environment of sedimentary basins [7]. As regards the speed of the tectonic plates motion, Cloetingh et al. [8] pointed out that 10 mm/yr is a characteristic velocity of oceanic lithospheres, while Assaad [9] indicated that the average movement rate of tectonic plates is around 1 to 2 mm/yr currently.

Few works have been recently dedicated to theoretical or numerical modeling of these phenomena. Zhao et al. [10] developed a finite element model to simulate the fluid rock interaction in pore-fluid saturated hydrothermal sedimentary basins. A numerical model was proposed in [11] that aimed to simulate the distribution of seafloor geotechnical parameters during the growth of a seismically active continental margin.

Disregarding the chemical aspects, the present work is devoted to purely mechanical modeling of compaction in sedimentary basins by means of numerical simulations performed in a two-dimensional setting. The finite element approach is developed to simulate the sediments deposition and the mechanical processes involved during the formation of a sedimentary basin in a saturated environment. One of the major difficulties involving this kind of simulation is connected with the occurrence of large change in porosity throughout the compaction process. The coupled nature of the deformation problem may be understood as follows: large strains modify the microstructure, which leads to a change in the poromechanical properties of the sediment material and thus affecting the basins response. This behavior requires that the poromechanical constitutive law be formulated in the framework of finite irreversible strains, so the key components for the model are the hydromechanical and elasticity-plasticity couplings. Another specificity of the present problem is that sedimentary basins simulations deal with open material systems. A finite element technique developed in [12], which is specifically devised for simulating the processes of sediment accretion, is adopted in the present analysis.

Particular emphasis is given to the investigation of tectonic-driven deformation in sedimentary basins caused by extensional and compressive movements. The simulations are performed reasoning on a rectangular geometrical model that is intended to represent an oceanic trench created by pre-depositional divergent tectonics. Then, sediment accumulation occurs over tens of millions of years. After the period of deposition and compaction of the sediments resulting from gravitational forces and pore-pressure dissipation, tectonic movements are applied on the sides of the basin. The sedimentary rock is modeled as a fully saturated poroelastoplastic material undergoing large strains.

2 GOVERNING EQUATIONS

At the macroscopic scale, a porous medium can be viewed as the superposition of a solid continuum related to the deformable skeleton and a fluid phase occupying the porous space. In this approach, the amount of fluid content within an infinitesimal volume of porous material $d\Omega_t$ is represented by the porosity. The Lagrangian porosity ϕ is defined by the ratio between the fluid volume in the current configuration (represented by the superscript *f*) and the initial total volume, $\phi = d\Omega_t^f / d\Omega_0$, while the Eulerian porosity φ quantifies the fluid content with respect to the current total volume, $\varphi = d\Omega_t^f / d\Omega_t$.

Therefore, in order to define the poromechanical problem under isothermal and quasi-static conditions, two field equations referring to momentum and mass balance over the space where the problem takes place must be specified. By considering the balance of linear momentum, the equilibrium equation for the porous continuum can be obtained:

$$div\underline{\underline{\sigma}} + \rho \underline{g} = \underline{0} \tag{1}$$

where $\underline{\underline{\sigma}}$ is the Cauchy total stress tensor, $\underline{g}$ is the acceleration of gravity and ρ is the porous material density, defined by the Eulerian porosity, the fluid density ρ^f and the grain density ρ^s:

$$\rho = \varphi\rho^f + (1-\varphi)\rho^s \tag{2}$$

The second field equation is the fluid mass balance (3), function of the filtration vector $\underline{q}$ defined by Darcy's law (4), where *J* is the Jacobian of the transformation, *p* is the pore-pressure and $\underline{\underline{k}}$ is the permeability tensor (in case of isotropy, $\underline{\underline{k}} = k\underline{\underline{1}}$).

$$\frac{d}{dt}\left(\rho^f \phi\right) + J div\left(\rho^f \underline{q}\right) = 0 \tag{3}$$

$$\underline{q} = \underline{\underline{k}}.\left(-\nabla p + \rho^f \underline{g}\right) \tag{4}$$

The problem is completely defined only when the geometry and the values of all corresponding fields are specified at the initial moment. For the boundary conditions in the current configuration t, partitions of the boundary $\partial\Omega_t$ of the geometrical domain Ω_t are introduced. The directions in which the boundary conditions are applied are defined by the unit normal vector $\underline{n}$ and two perpendicular directions. The data are indicated by the superscript d. Let $\underline{\xi}$ be the total displacement vector of a skeleton particle, $\underline{T}$ be the stress vector and $\underline{e}_i$ be the unit director vectors for the coordinate system *(i = 1,2,3)*.

For the mechanical boundary conditions, let S^{Ti} and $S^{\xi i}$ be the parts of $\partial\Omega_t$ where the ith component of the stress and displacement vectors are imposed. Expressions below must be satisfied, where $\left(\underline{\underline{\sigma}}.\underline{n}\right).\underline{e}_i = T_i = T_i^d$ on S^{Ti}, and $\underline{\xi}.\underline{e}_i = \xi^d$ on $S^{\xi i}$.

$$S^{Ti} \cup S^{\xi i} = \partial\Omega_t \qquad\qquad S^{Ti} \cap S^{\xi i} = \varnothing \tag{5}$$

For the hydraulic boundary conditions, let S^W and S^P be the parts of $\partial\Omega_t$ where the normal component of the fluid mass flux and the fluid pressure are imposed, respectively. We have:

$$S^W \cup S^P = \partial\Omega_t \qquad\qquad S^W \cap S^P = \varnothing \tag{6}$$

where $\underline{w}.\underline{n} = w^d$ on S^W, and $p = p^d$ on S^P.

The macroscopic equations of state of a fully saturated poroelastoplastic material generally assume a total independence of the elastic properties with respect to the plastic behavior. However, in the context of large strains, such an assumption is clearly questionable as the large macroscopic plastic strains are associated with an irreversible evolution of the microstructure, which is responsible for variations of the macroscopic elastic properties of the porous medium [13].

The idea of the constitutive model here presented consists in associate the evolution of the elastic and hydraulic properties of the porous material to its variation of porosity, which is associated to the plastic part of the Jacobian of the transformation. We shall refer to this phenomenon as elasticity–plasticity coupling.

Let us consider a representative elementary volume (r.e.v.) of the porous medium subjected to a stress state $\underline{\underline{\sigma}}$ and pore-pressure p. Removing this load applied to the initial configuration $d\Omega_0$, the actual volume $d\Omega_t$ transforms to a residual configuration $d\Omega_u$. This transformation between $d\Omega_t$ and $d\Omega_u$ is referred to as the elastic part. The variation of the elastic porosity and the plastic porosity are defined as:

$$\phi^{el} = \frac{\left|d\Omega_t^f\right| - \left|d\Omega_u^f\right|}{\left|d\Omega_u\right|} \qquad\qquad \phi^p = \frac{\left|d\Omega_u^f\right| - \left|d\Omega_0^f\right|}{\left|d\Omega_0\right|} \tag{7}$$

If $\underline{\underline{F}}^{\mathrm{el}}$ is the gradient of the homogenous geometric transformation of a skeleton particle between $d\Omega_u$ and $d\Omega_t$, and $\underline{\underline{F}}^p$ is the gradient of the homogenous geometric transformation of a skeleton particle between $d\Omega_0$ and $d\Omega_u$, the gradient $\underline{\underline{F}}$ is given by:

$$\underline{\underline{F}} = \underline{\underline{F}}^{el}.\underline{\underline{F}}^{p} \tag{8}$$

The plastic part of the Jacobian of the transformation J^p being defined as $J^p = d\Omega_u / d\Omega_0 = det\underline{\underline{F}}^p$, the variation of porosity is described as follows:

$$\phi - \phi_0 = \phi^p + J^p \phi^{el} \tag{9}$$

Figure 1 illustrates the decomposition of the gradient $\underline{\underline{F}}$ and the variation of porosity experienced by the porous material.

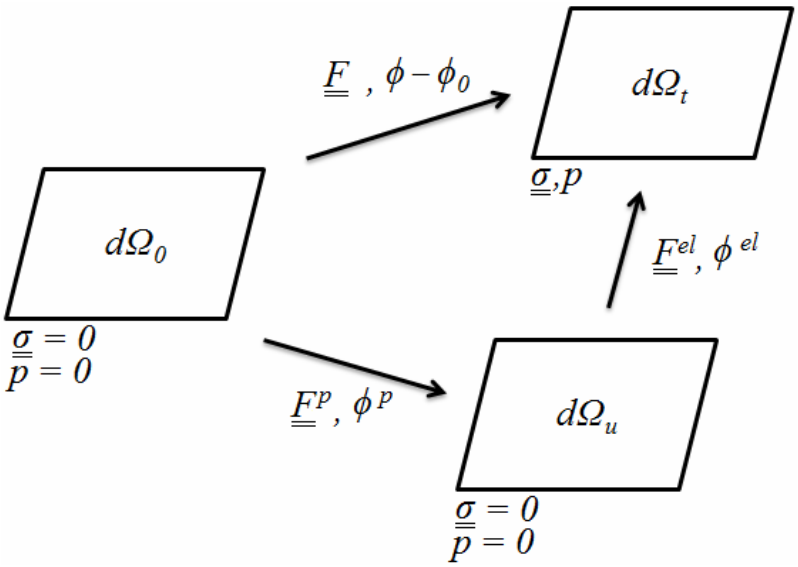

Figure 1: decomposition of the gradient of transformation and variation of porosity.

The elastic part of the transformation between $d\Omega_u$ and $d\Omega_t$ is assumed infinitesimal, $\underline{\underline{F}}^{el} \approx 1$. The state equations for linear elasticity are simply given according to Biot's theory for isotropic materials:

$$\underline{\underline{\sigma}} = \underset{\sim}{C} : \underline{\underline{\varepsilon}}^{el} - \underline{\underline{B}} p \tag{10}$$

$$p = M\left(\phi^{el} - \underline{\underline{B}} : \underline{\underline{\varepsilon}}^{el}\right) \tag{11}$$

where $\underline{\underline{\varepsilon}}^{el}$ stands for the infinitesimal elastic strain associated with the elastic sequence $\underline{\underline{F}}^{el}$, $\underline{\underline{B}}$ and M are respectively the Biot tensor and Biot modulus, and $\underset{\sim}{C}$ is the fourth order tensor of the drained elastic moduli:

$$\underset{\sim}{C} = \left(K - 2\mu/3\right)\ \underline{\underline{1}} \otimes \underline{\underline{1}} + 2\mu\ \underset{\sim}{1} \tag{12}$$

The main difference with the usual Biot's theory lies in the fact that the state variables $\underline{\underline{\varepsilon}}^{el}$ and ϕ^{el} are here defined with respect to the unstressed configuration. So as the porous medium deforms reducing its porosity, the evolution of the elastic properties (the bulk and shear moduli of the porous material, K and μ) are evaluated by the Hashin-Shtrikman upper bounds [14], function of the bulk and shear moduli of the solid phase k^s and μ^s as well as of the Eulerian porosity φ:

$$K(\varphi) = \frac{4k^s\mu^s(1-\varphi)}{3k^s\varphi + 4\mu^s} \tag{13}$$

$$\mu(\varphi) = \frac{\mu^s(1-\varphi)\left(9k^s + 8\mu^s\right)}{k^s(9+6\varphi) + \mu^s(8+12\varphi)} \tag{14}$$

Under isotropy conditions, classical results of poroelasticity indicate that:

$$\underline{\underline{B}} = b\underline{\underline{1}} \quad \text{with} \quad b(\varphi) = 1 - \frac{K(\varphi)}{k^s} \quad \text{and} \quad \frac{1}{M(\varphi)} = \frac{b(\varphi) - \varphi}{k^s} \tag{15}$$

The effects of microstructural changes on the evolution of the permeability coefficient of the porous medium k may be modeled by means of the Kozeny–Carman formula:

$$\underline{\underline{k}} = k\underline{\underline{1}} \quad \text{with} \quad k(\varphi) = k_0 \frac{\varphi^3 (1-\phi_0)^2}{\phi_0^3 (1-\varphi)^2} \tag{16}$$

In the framework of finite poroplasticity, considering the evolution of the poromechanical properties, the macroscopic rate equations of state take the following rate form [13]:

$$\frac{D_J \underline{\underline{\sigma'^e}}}{Dt} = \dot{\underline{\underline{\sigma}}}'^e + \underline{\underline{\sigma}}'^e . \underline{\underline{\Omega}} - \underline{\underline{\Omega}} . \underline{\underline{\sigma}}'^e = \underset{\sim}{C} : \left(\underline{\underline{d}} - \underline{\underline{d}}^p \right) + \dot{\underset{\sim}{C}} : \underset{\sim}{C}^{-1} : \underline{\underline{\sigma}}'^e \tag{17}$$

$$\dot{p} = M \left(-b \mathrm{tr}\left(\underline{\underline{d}} - \underline{\underline{d}}^p \right) + \frac{\dot{\phi} - \dot{\phi}^p}{J^p} \right) + \frac{\dot{M}}{M} p - M\dot{b} \mathrm{tr}\left(\underset{\sim}{C}^{-1} : \underline{\underline{\sigma}}'^e \right) \tag{18}$$

where $\underline{\underline{\sigma}}'^e = \underline{\underline{\sigma}} + \underline{\underline{B}} p$ is the Biot effective stress, $\underline{\underline{\Omega}}$ is the spin tensor and $\underline{\underline{d}}^p = \left\{ \dot{\underline{\underline{F}}}^p . \left(\underline{\underline{F}}^p \right)^{-1} \right\}_{sym}$ is the plastic strain rate.

Introducing the plastic potential $G(\underline{\sigma}')$ which depends on $\underline{\sigma}$ and p through the Terzaghi effective stress $\underline{\underline{\sigma}}' = \underline{\underline{\sigma}} + p\underline{\underline{1}}$, where $\dot{\chi}$ is a non-negative plastic multiplier:

$$\underline{\underline{d}}^p = \dot{\chi} \frac{\partial G}{\partial \underline{\underline{\sigma}}'} \tag{19}$$

The plastic model used here is the modified Cam-Clay model [15]. The plastic flow rule is associated. The yield surface f is function of the deviatoric stress tensor $\underline{s}$ and the mean effective stress p' defined as:

$$\underline{\underline{s}} = \underline{\underline{\sigma}} - \frac{1}{3} tr\left(\underline{\underline{\sigma}} \right) \underline{\underline{1}} \qquad p' = \frac{1}{3} tr\left(\underline{\underline{\sigma}}' \right) \tag{20}$$

The plastic criterion is then:

$$f\left(\underline{\underline{\sigma}}', p_c \right) = \frac{3}{2} \underline{\underline{s}} : \underline{\underline{s}} + M_{cs}^2 p' \left(p' + p_c \right) \tag{21}$$

where M_{cs} is the slope of the critical state line and p_c is the consolidation pressure, which represents the hardening parameter of the considered model. Its evolution with the volume plastic strains is the hardening law. The latter has been derived from a micromechanics-based reasoning developed in Barthélémy et al. [16]:

$$p_c\left(J^p \right) = \frac{p_{co}}{\ln \phi_0} \ln\left(1 - \frac{1 - \phi_0}{J^p} \right) \tag{22}$$

As observed in Deudé et al. [17], the main advantage of the above hardening law with respect to classical ones lies in the fact that it avoids the development of negative porosities under high isotropic compression.

3 FINITE ELEMENT DISCRETIZATION

Assessment of the poromechanical state requires the determination of the temporal evolution of the geometric transformation as well as the pore-pressure changes. This shall be achieved by solving the boundary value problem defined by the set of governing equations together with the constitutive and complementary equations. The particularity of large strains is that all equations actually refer to the mechanical system in its current configuration, which is a priori unknown. The finite element procedure used for assessing the evolution of stresses, pore pressures and strains in the porous medium under consideration will be outlined hereafter. Full details are provided in Bernaud et al. [13].

The analysis is based on the implementation of the updated Lagrangian scheme [18]. This approach is based on the same procedures used by total Lagrangian formulations, but instead of being referred to the initial configuration, all static and kinematic variables are referred to the last calculated configuration, say at time t. The unknown variables are then updated in each step time Δt. The displacement $\underline{U}$ of the skeleton particles between t and $t+\Delta t$ is defined as

$$\underline{U} = \underline{x}^{t+\Delta t} - \underline{x}^{t} \tag{23}$$

where $\underline{x}^{t}$ (resp. $\underline{x}^{t+\Delta t}$) denotes the coordinate of the particle at time t (resp. $t+\Delta t$). The pore pressure difference at points similar within the skeleton transformation between t and $t+\Delta t$ is

$$P = p(\underline{x}^{t+\Delta t}) - p(\underline{x}^{t}) \tag{24}$$

The discretized form of the problem is obtained from weak formulation of the equilibrium and fluid mass balance equations at time $t+\Delta t$. Six-nodes triangles are used for geometry discretization (figure 2). A piecewise quadratic polynomial function is adopted to approximate the displacement, while piecewise linear function is adopted for pore-pressure variations.

The resulting system is given below, where $\boldsymbol{K}_{IJ}$ are the global stiffness sub-matrices and $\underline{F}_I$ the global force sub-vectors. $\underline{U}$ and $\underline{P}$ are the nodal displacements and pore-pressure difference, respectively. For a single element, $\boldsymbol{K}_{UU}$ is a 12×12 matrix, $\boldsymbol{K}_{PU}$ is 12×3, $\boldsymbol{K}_{UP}$ 3×12 and $\boldsymbol{K}_{PP}$ 3×3, resulting in a 15×15 stiffness matrix.

$$\begin{bmatrix} \boldsymbol{K}_{UU} & \boldsymbol{K}_{PU} \\ \boldsymbol{K}_{UP} & \boldsymbol{K}_{PP} \end{bmatrix} \begin{bmatrix} \underline{U} \\ \underline{P} \end{bmatrix} = \begin{bmatrix} \underline{F}_U \\ \underline{F}_P \end{bmatrix} \tag{25}$$

It is emphasized that, for a given configuration at time t, the system above is highly non-linear due to the physical non-linearities (plasticity) and geometrical non-linearities (large strains). In particular, vectors $\underline{F}_U$ and $\underline{F}_P$ depend on the unknowns $\underline{U}$ and $\underline{P}$. An iterative method is adopted for solving this system by implementing an appropriate algorithms until it is satisfied up to a required tolerance.

One specificity of the problem lies in the fact that a sedimentary basin is an open system due to the continuous accretion of material at the top of the basin during sedimentation phase. This requires an appropriate technique to overcome the difficulty of dealing with an open system in the context of finite element method. For this purpose, the activation/deactivation method [12] inspired from tunnel engineering is used to simulate the accretion process. In the framework of such method, the real open material system is simulated as fictitious closed one.

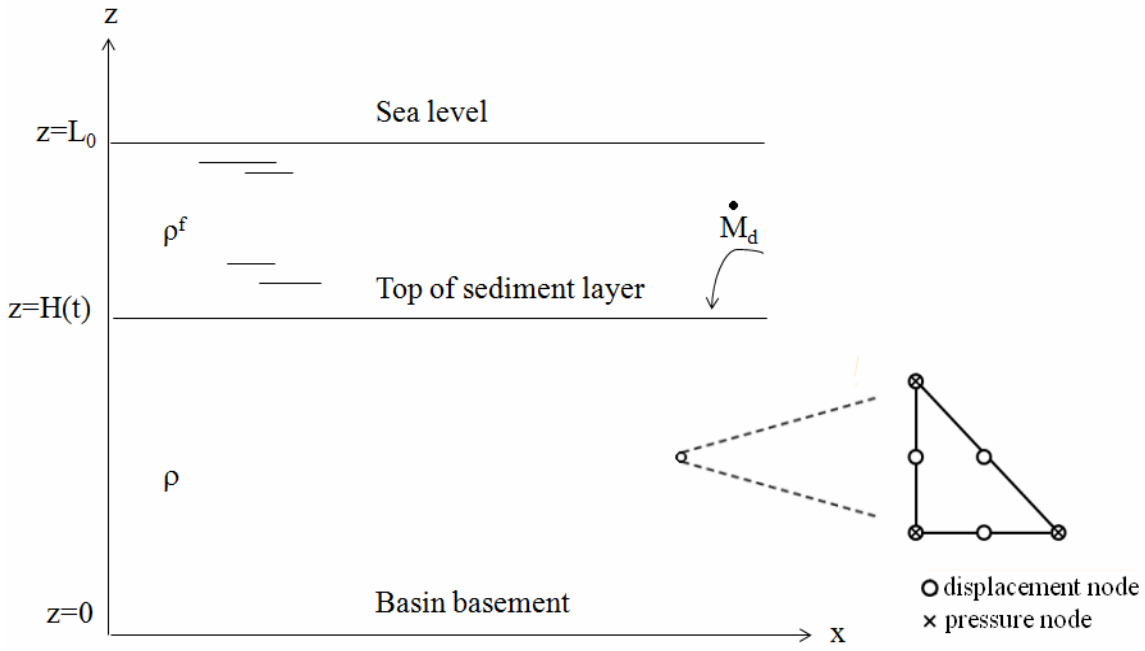

Figure 2: Schematic geometry of the basin and the finite element characteristics.

Figure 2 illustrates the basin construction problem, where L_0 corresponds to the sea level and $H(t)$ corresponds to the top of the sediment layer. The evolution in time of the latter must of course correspond to that of the real system. If $\rho(z,t)$ represents the mass density of the sedimented material, the total sediment mass per unit area provided from the initial moment $t = 0$ is equal to the mass of the vertical column with unit cross section of equation (26):

$$M_d(t) = \int_0^{H(t)} \rho(z,t)\,dz \tag{26}$$

Based on this reasoning, the height of a given layer of sediments deposited between the times $t = 0$ and $t = T$ can be defined using equation (27), where $\rho_0(t)$ is the sediments initial density at the corresponding time t.

$$H = \int_0^T \frac{\dot{M}_d(t)}{\rho_0(t)}\,dt \tag{27}$$

In fact, H represents the thickness of the layer that was deposited in the basin up to time T if the deposited material was rigid. However, while sediments layers are being applied, the already deposited layers are in compaction process. The simulation of the accretion phase takes place subdividing the sedimentation period into n subintervals $[t_{i-1}, t_i]$ with $t_0 = 0$ and $t_n = T$. During the time increment $\Delta t_i = t_i - t_{i-1}$, the addition of sediments corresponds to a height of ΔH:

$$\Delta H_i = \int_{t_{i-1}}^{t_i} \frac{\dot{M}_d(t)}{\rho_0(t)}\,dt \tag{28}$$

Before sediment deposition, all finite element layers constituting the system are attributed the sea water properties. For every advanced subinterval Δt, the properties of a corresponding layer with thickness ΔH are changed in conjunction with the hydraulic and elastic properties of the deposited material. This process starts at the bottom of the basin $(z = 0)$ and continues upwards until the accretion phase ends.

4 COMPUTATIONAL RESULTS

The sedimentary basin considered in the numerical simulation is formed during $T = 60$ millions years (duration of accretion phase). In addition, the rate of sediment accretion is constant and equal to $\dot{M}_d = 4.34 \times 10^{-9}$ kg/s per unit area, corresponding to 100 m of sediment thickness per million years in unloaded conditions. In absence of compaction, that is if the sediment material were rigid, the total thickness of the basin would be 6 km at $t = T$ (end of accretion phase).

The simulations of the sedimentary basin are performed considering three distinct phases defined as follows. Phase (1): corresponds to sediment deposition (formation of the basin) that extends from $t = 0$ and $t = T$. Phase (2): compaction exclusively due to gravitational forces and pore-pressure dissipation. Phase (3): lateral movement induced by extensional or compressive tectonic events.

The initial geometry of the basin is sketched in Figure 3. It consists in a rectangular block of 24 km long by $H = 6$ km thick. Owing to the symmetry with respect to the vertical plane, only the half part of the geometrical domain is discretized into finite elements. The finite element mesh consists in 7200 triangular elements regularly distributed along 120 horizontal layers, each layer being divided into 60 elements. The mesh corresponds to 14701 total nodes.

The model data are: initial material density $\rho_0 = 1.37 \times 10^3$ kg/m^3, initial porosity $\phi_0 = 0.72$ (taken from [19]), initial Young modulus $E_0 = 10^3$ MPa, initial Poisson's ratio $\nu_0 = 0.33$, initial Biot coefficient $b_0 = 0.9715$, initial Biot modulus $M_0 = 1.392 \times 10^5$ MPa, coefficient slope of the critical state line $M_{cs} = 1.2$, initial permeability $k_0 = 10^{-10}$ MPa^{-1} m^2 s^{-1}, initial consolidation pressure $p_{co} = 1.5$ MPa, sea water density $\rho^f = 10^3$ kg/m^3.

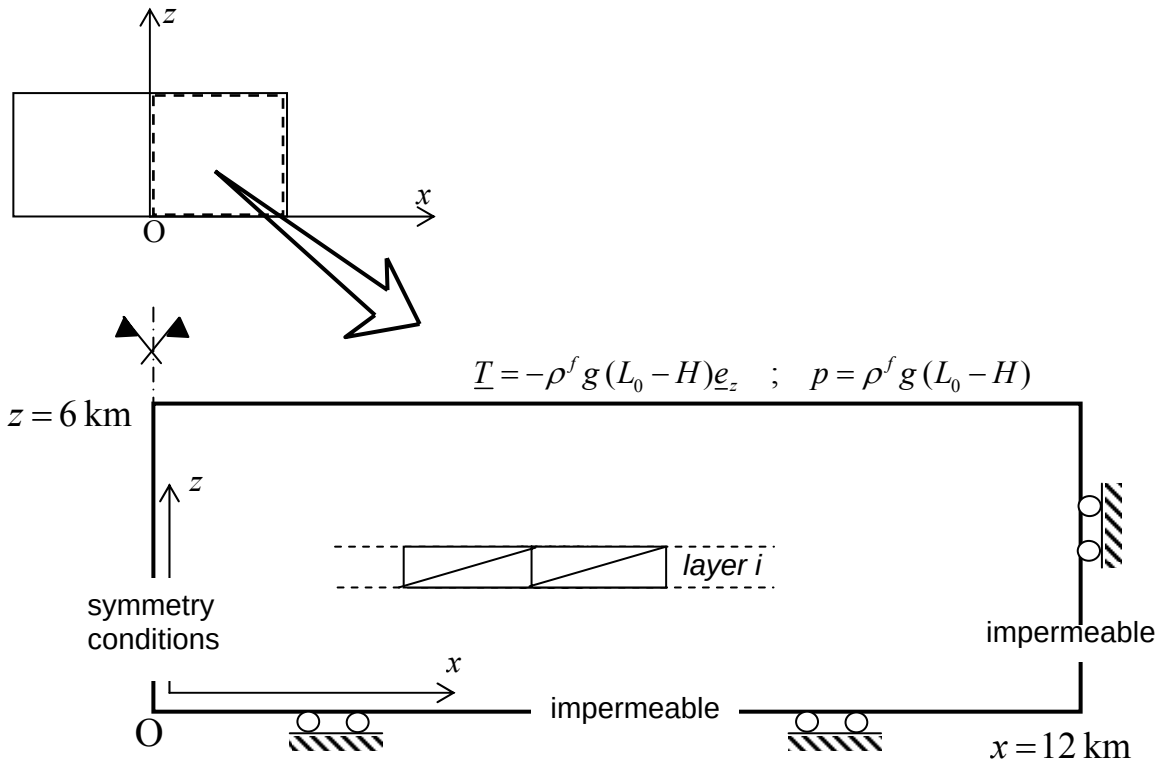

Figure 3: basin configuration.

The boundary conditions applied to geometric domain are:

z = H(t) (upper surface):

$$\underline{T} = -\rho^f g\left(L_0 - H\left(t\right)\right)\underline{e}_z \qquad p = \rho^f g\left(L_0 - H\left(t\right)\right) \tag{29}$$

z = 0 (basin basement):

$$\underline{\xi}.\underline{e}_z = 0 \qquad \underline{q}.\underline{e}_z = 0 \tag{30}$$

x = 12 km (basin side):

$$\underline{\xi}.\underline{e}_x = 0 \qquad \underline{q}.\underline{e}_x = 0 \tag{31}$$

The above boundary conditions are completed by symmetry conditions at plane $x = 0$.

4.1 Gravitational compaction

Figure 4 illustrates the compaction law of the sedimentary basin along phases (1) and (2). As it can be seen, the thickness of the basin is about H = 4212 m at the end of accretion phase (T = 60 millions years), which represents a compaction level of 30%. At t = 60T, the thickness of the basin is almost stabilized with H = 2633 m, corresponding to 56% compaction level. Based on this compaction law, five different ages of the basin have been chosen to apply laterally-induced tectonic deformations (i.e., phase (3)). The selected basin ages are indicated in Figure 4 and given in Table 1 together with corresponding basin thickness.

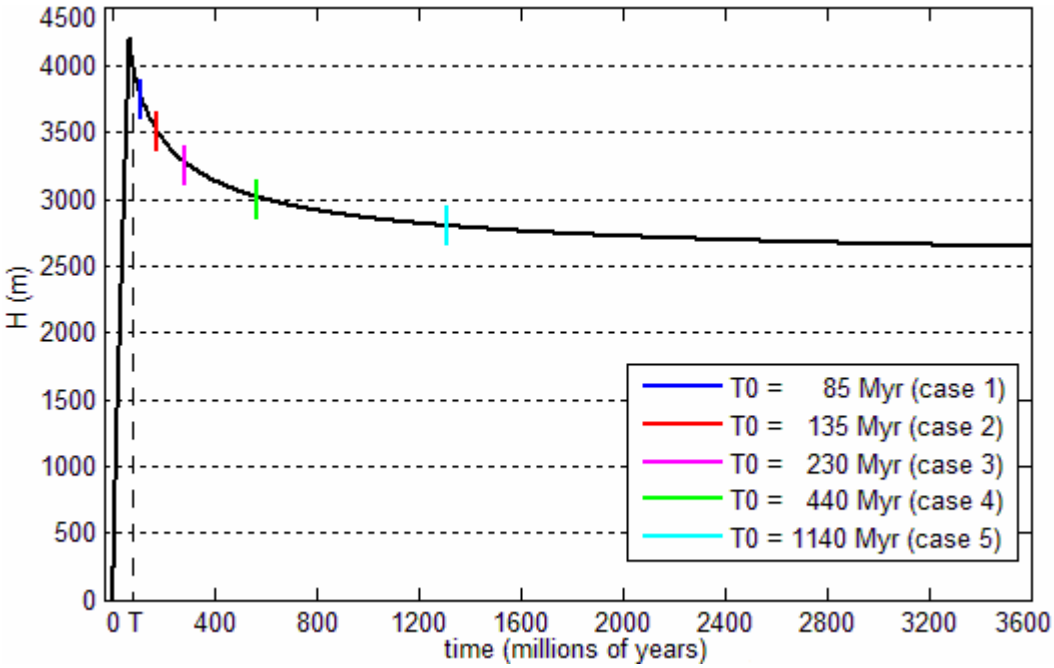

Figure 4: Compaction law of the sedimentary basin.

Case	Height (m)	Age (myr)
1	3750	85
2	3500	135
3	3250	230
4	3000	440
5	2750	1140

Table 1: selected cases.

Before presenting the simulation of tectonic sequences, some results related to phases (1) and (2), which correspond to oedometric compaction, shall be analyzed hereafter. The pore-pressure profile is displayed in figure 5 for each referred case. The hydrostatic pore-pressure profile is drawn as well. It can be seen that although case $t = 60T$ is nearly asymptotic in relation to its compaction history (figure 4), the pore-pressure profile is still far from hydrostatic. The Kozeny-Carman formula used to quantify the evolution of the permeability coefficient indicates that $k \to 0$ when $\varphi \to 0$. This explains the long time required for total dissipation of excess pore-pressure in the lower layers of the basin, i.e. the time required to attain the asymptotic state of the basin.

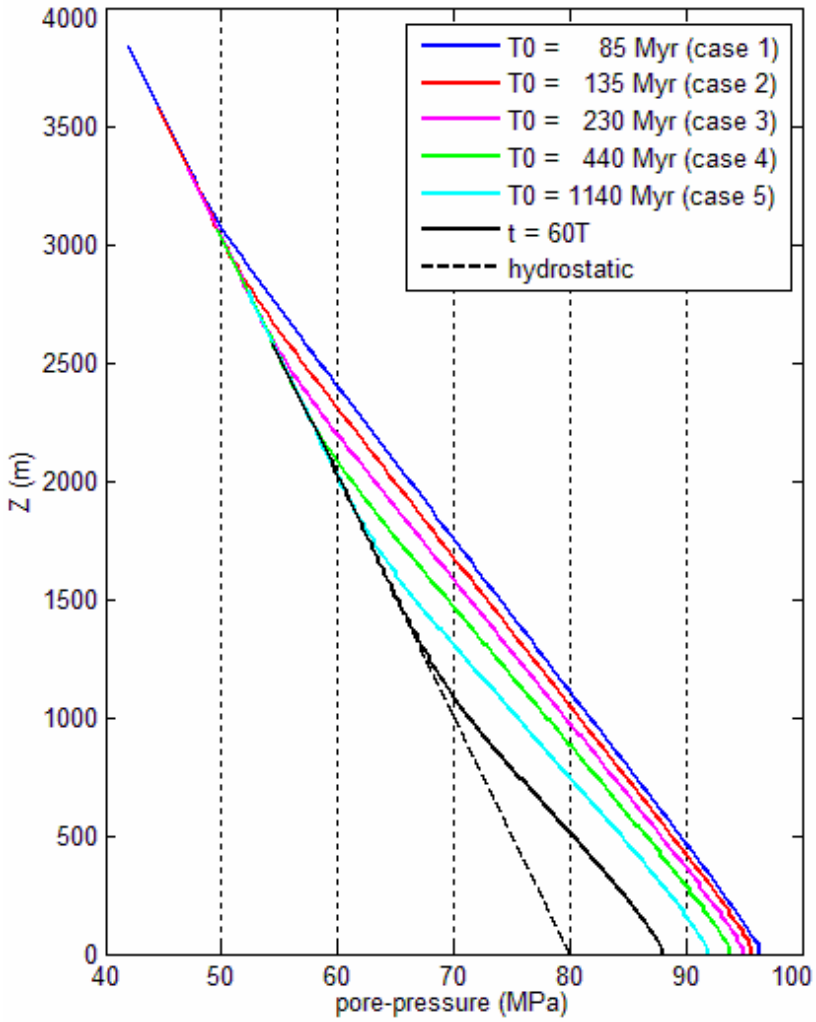

Figure 5: Pore-pressure profiles during gravitational compaction.

The porosity profiles are shown in figure 6. As expected, younger sedimentary basins present higher porosities along their height, since excess pore-pressure is continuously dissipated in course of time, leading the sediment layer to compaction as the fluid is expelled from the porous material. The $t = 60T$ case porosity in the lower layers vary from 7% to 17%. These small values explain the difficulty to continue its gravitational compaction as commented above, since the permeability in these layers are 10 to 100 times lower than its initial value.

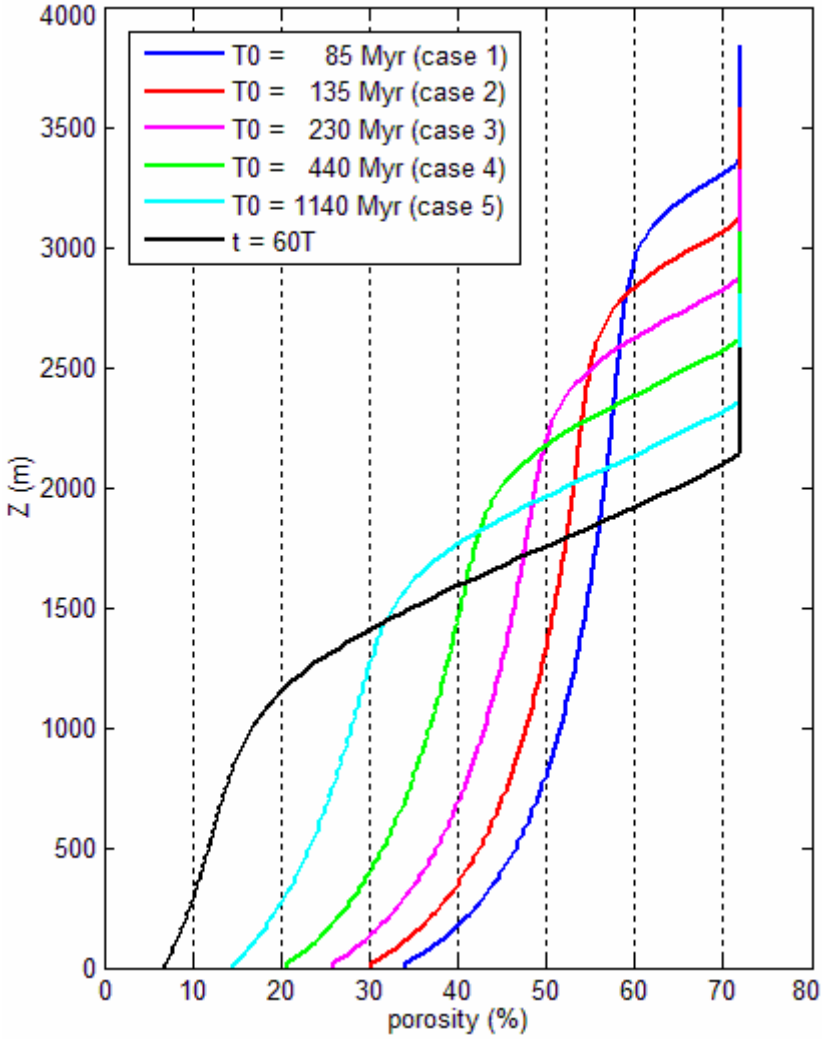

Figure 6: Porosity profiles during gravitational compaction.

In classical analysis of soil mechanics, an important parameter is the coefficient of earth pressure *Kp*, defined as the ratio between the horizontal and vertical effective stresses $Kp = \sigma'_H / \sigma'_V$. This parameter is often considered constant along the depth of a basin. Its estimation allows access to the horizontal effective stress profiles based on the vertical effective stress obtained from traditional analysis of one-dimensional calculations. Indeed, the obtained values of *Kp* coefficient before tectonic motion are constant for all cases along basins depth, except within a thin crust located near the upper surface of the basin as can be seen in figure 7.

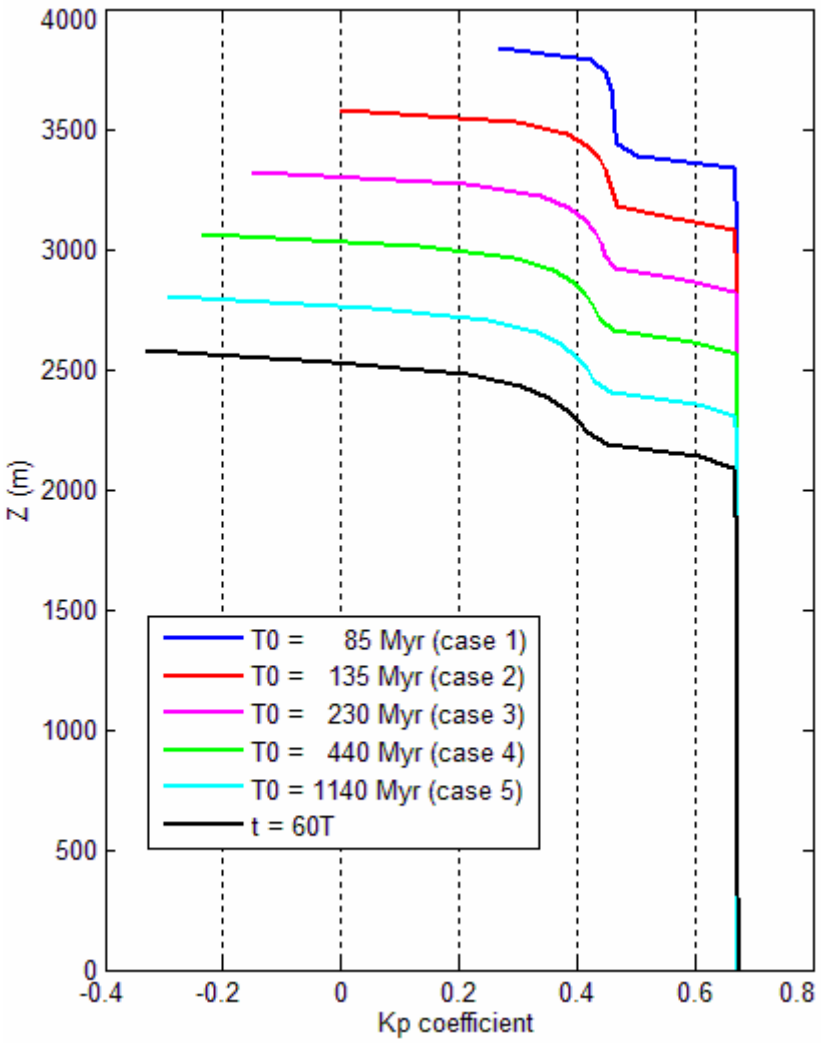

Figure 7: Profiles of coefficient Kp during gravitational compaction.

4.2 Tectonic sequences

For each one of the five selected ages, a tectonic loading is applied by imposing at $t = T_0$ a lateral movement to the basin. In each case, the geometry and hydromechanical fields (stress, pore pressure, porosity and associated poromechanical parameters) resulting from phases (1) and (2) are considered as the initial configuration and state of the basin when starting the tectonic loading. The hydromechanical boundary conditions are showed in Figure 8. The lateral right-hand side (resp. left-side) is subjected to a constant horizontal velocity $V\,\underline{e}_x$ (resp. $-V\,\underline{e}_x$). We restrict the analysis to a prescribed velocity magnitude $V = 1\,\text{mm}/\,\text{year}$, which falls within the category of slow tectonics. The lateral displacement is applied using time increment of $\Delta t = 1\,\text{year}$.

Tectonic sequences have been simulated in the five cases defined in Table 1. For each case, the total lateral displacement applied to the basin before the numerical failure of the plasticity algorithm was equal to $\pm 1200\,\text{m}$. This means that the total duration of tectonic sequences is about 1.2 million of years.

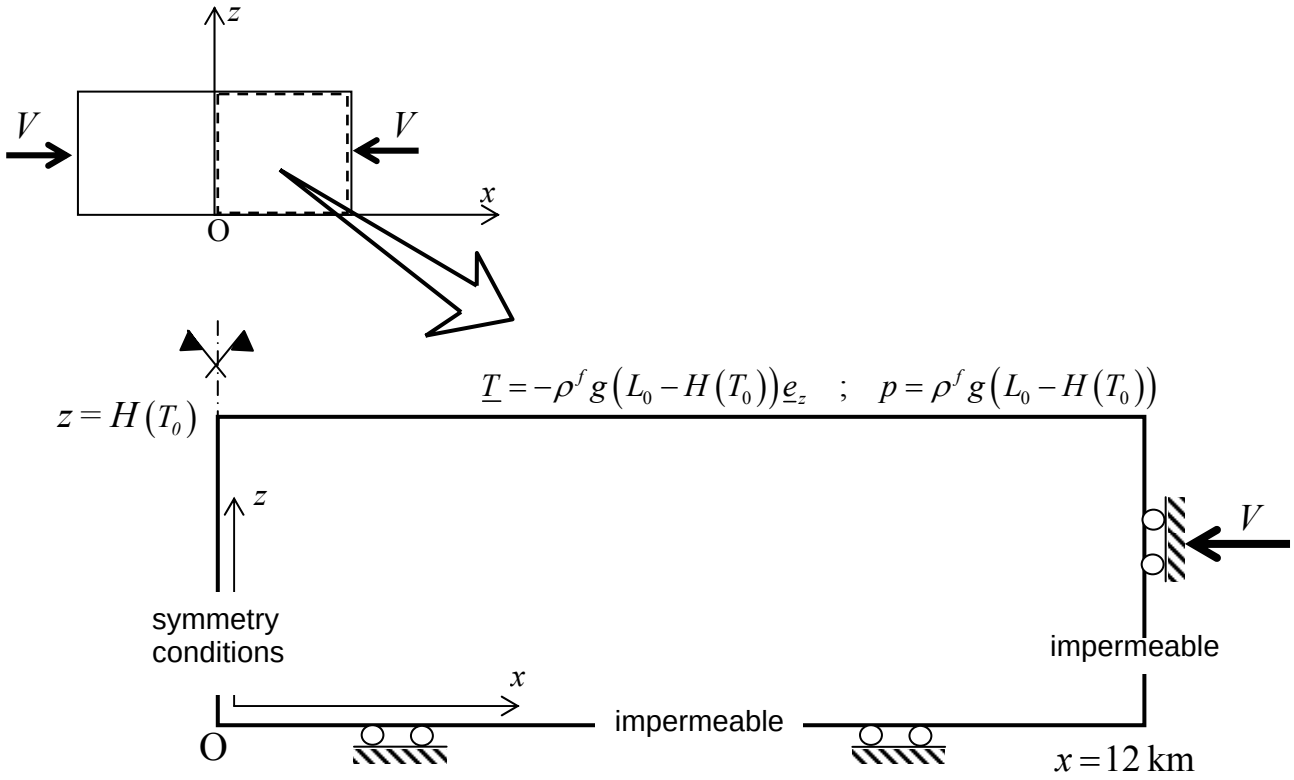

Figure 8: Geometrical model and boundary conditions for tectonic simulations.

The first observation made from the numerical simulations is that the configurations reached by the basins at the end of tectonic sequences are almost the same for all considered cases of extensional solicitation. The same can be said for all case of compressive solicitation. However, the final configurations in extensional or compressive solicitation are distinct. Hence, for sake of clearness, only the results related to the case 1 will be presented in the sequel. It is recalled that the case 1 is defined by a tectonic loading starting at T_0=85 Myr and associated to an initial basin thickness $H(T_0)$=3750 m .

Figure 9 shows the thickness of the basin versus time for $T_0 \le t \le T_0 + 1.2$ Myr . An important feature raised from the numerical simulations is that the lateral solicitation strongly affects the velocity of the compaction process in both extensional and compressive situations. As a matter of fact, after 1.2 million of years the basin compacted only 10 m under gravitational compaction, while after the same period it compacted more than 1500 m under extensional lateral motion and more than 1200 m under compressive lateral motion.

The distribution of pore-pressure along the right side of the basin after 1.2 Myr is displayed in Figure 10 for the case 1. The compressive tectonic motion led to a substantial increase in the pore-pressure profile, reaching about 20 MPa of excess pore-pressure in the basin basement, while the extensional tectonic accelerated the process of dissipation of the excess pore-pressure.

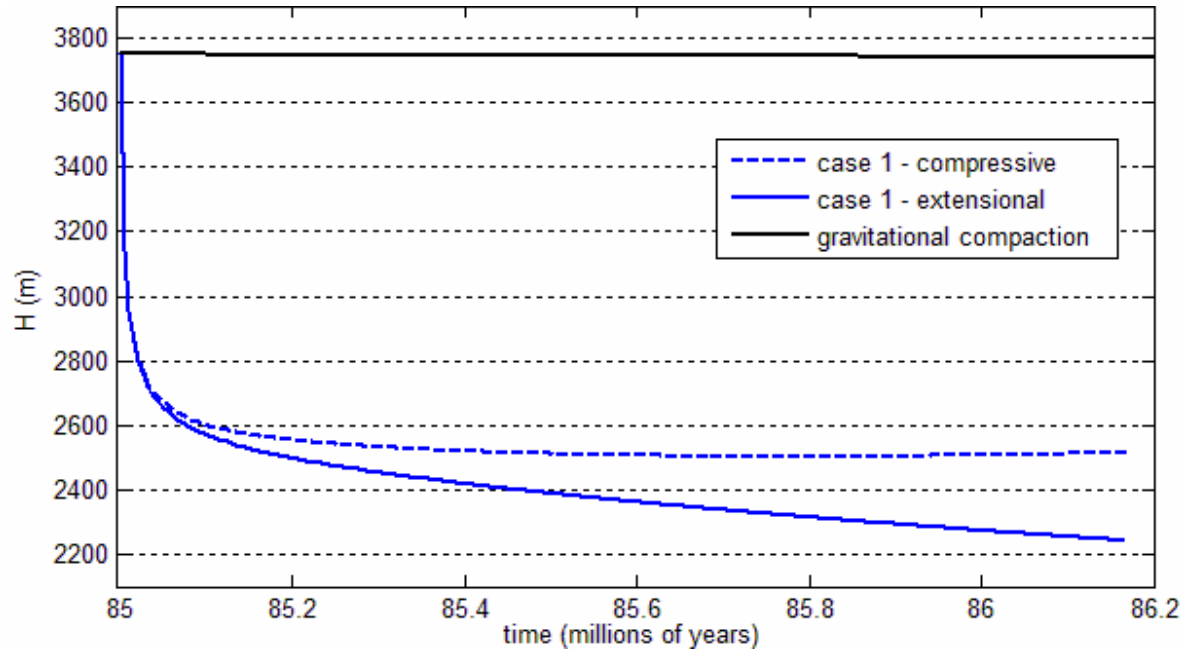

Figure 9: Influence of tectonic lateral motion on the compaction law.

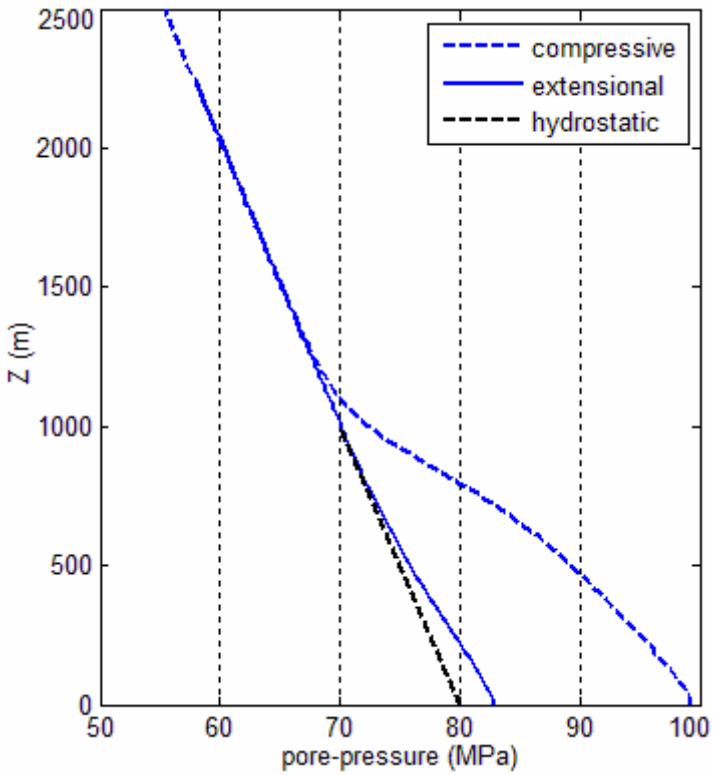

Figure 10: Pore-pressure profile along the right side of the basin after 1.2 Myr tectonic loading.

Figures 11 and 12 present respectively the porosity and coefficient *Kp* along the right side of the basin. Even induced by distinct driven mechanisms, the expulsion of pore-fluid in both cases led to a significant decrease in the sediment layer porosity, reaching the quasi total closure of pores near the basin basement. Regarding coefficient *Kp* of earth pressure, it turns out that this coefficient is uniform along the basin thickness for the extensional case, similarly to what has been observed

under purely gravitational compaction (phases (1) and (2)). In contrast, the distribution along the basin thickness is quite disturbed for the compressive case.

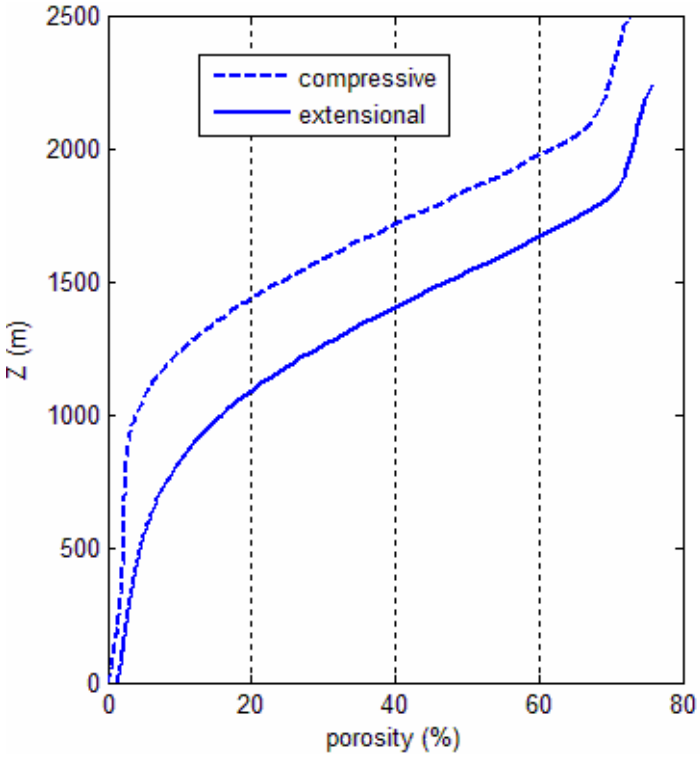

Figure 11: Porosity profile along the right side of the basin after 1.2 Myr tectonic loading.

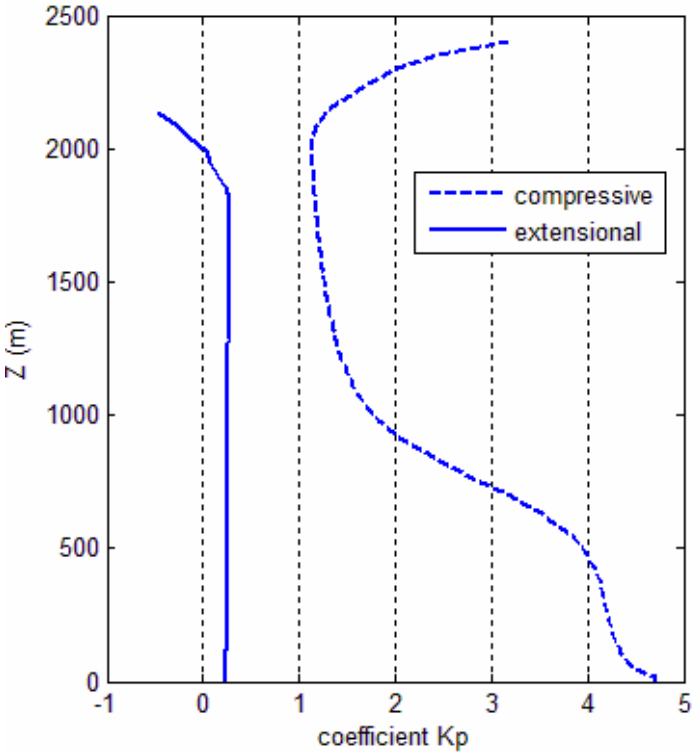

Figure 12: Profile of coefficient *Kp* along the right side of the basin after 1.2 Myr tectonic loading.

5 CONCLUSIONS

Starting from the constitutive model developed by Bernaud et al. [13] in the context of finite poroplasticity, three important phases involved in the mechanical processes of a sedimentary basin formation were simulated: the sediments accretion phase, its compaction due to gravitational forces and pore-pressure dissipation, and the deformations imposed by compressive and extensional tectonics.

From the numerical point of view, the finite element model has been applied to the simulation within a 2D setting of both gravitational compaction and tectonic-induced deformation. The behavior of the basin during the phases of sediment accretion and pore pressure dissipation is first investigated. Starting from the configuration reached by the basin at a given age, tectonic sequences have been then applied to the basin. The tectonic sequences are simulated by applying to the basin lateral extensional or compressive displacements.

Even though the numerical simulations have been performed in the particular situation of slow tectonics, some important features that are connected with the induced deformation are emphasized. It is worth noting that the objective of this preliminary analysis is only to investigate the feasibility of the 2D modeling and not to provide quantitative insights in the basin deformation under tectonic loading.

At this stage, some fundamental questions arise regarding the theoretical aspects and the numerical modeling. First, the frictionless boundary condition considered at the basin basement is not very realistic, leading to a more deformable block. A more realistic model for the interface between the basin and the rock basement such as the Coulomb friction law should be implemented. Second, the shape quality of the mesh elements resulting from compaction (vertical stretching) between $t = 0$ and $t = T_0$ that corresponds to the beginning of the tectonic loading phase is rather low: due to oedometric contraction, the elements become thin with high aspect ratio. This is clearly a possible source of numerical inaccuracies and can lead to non convergence of the non-linear algorithm. Third, regarding the simulation of deep oceanic basins, a more comprehensive model should take into account intergranular pressure-solution (IPS) mechanisms, since chemical compaction represents a major mechanism of deformation in the lower layers of this type of sedimentary basins. Fourth, it is also intended to perform simulations with fractured basins, since they occur in most real cases of sedimentary basins.

One should be cautious regarding the conclusions drawn from the numerical simulation since only very slow tectonics have been considered. It is likely that fast tectonics will induce high pore pressure within the basin. The later will thus deform under undrained-like conditions, which in turn lead rapidly to substantial increase in the effective stresses controlling the yield failure. Actually this kind of analysis requires a more robust algorithm to deal with the high non-linear problem.

Finally, several issues remain to be addressed on both theoretical and computational viewpoints. In first line, the development of an efficient numerical tool implementing robust algorithms specifically devised for handling finite poroplasticity problems and parallel computing that allows dealing with high number of degrees of freedom that are involved in a 3D modeling is in progress.

REFERENCES

[1] Leeder, M.R., 1999, *Sedimentology and sedimentary basins: from turbulence to tectonics*, Blackwell Science, Oxford.

[2] Taylor D.W., 1948, *Fundamentals of soil mechanics*, John Wiley, New York.

[3] Schmidt V.; McDonald D.A., 1979, *The role of secondary porosity in the course of sandstone diagenesis*, Aspects of Diagenesis, 26:175-207.

[4] Hubbert M.K.; Rubey W.W., 1959, *Role of fluid pressure in mechanics of overthrust faulting. I. Mechanics of fluid-filled porous solids and its application to overthrust faulting*, Geological Society of America Bulletin, 70(2):115-166.

[5] Smith J.E., 1971, *The dynamics of shale compaction and evolution of pore-fluid pressures*, Mathematical Geology, 3(3):239-263.

[6] Gibson R.E., 1958, *The progress of consolidation in a clay layer increasing with time*, Géotechnique, 8(4):171-182.

[7] Allen P.A.; Allen J.R., 2005, *Basin analysis: principles and applications*, 2nd ed. Blackwell Science, Oxford.

[8] Cloetingh S.A.P.L.; Wortel M.J.R.; Vlaar N.J., 1984, *Passive margin evolution, initiation of subduction and the Wilson Cycle*, Tectonophysics, 109:147-163.

[9] Assaad F.A., 2009, *Field Methods for Petroleum Geologists: A Guide to Computerized Lithostratigraphic Correlation Charts Case Study: Northern Africa*, Springer, Berlin.

[10] Zhao C.; Hobbs B.E.; Walshe J.L.; Mühlhaus H.B.; Ord A., 2001, *Finite element modeling of fluid–rock interaction problems in pore-fluid saturated hydrothermal/sedimentary basin*, Computer Methods in Applied Mechanics and Engineering, 190(18-19):2277-2293.

[11] Hutton E.W.H.; Syvitski J.P.M., 2004, *Advances in the numerical modeling of sediment failure during the development of a continental margin*, Marine Geology, 203(3-4):367-380.

[12] Bernaud D.; Dormieux L.; Maghous S., 2006, *A constitutive and numerical model for mechanical compaction in sedimentary basins*. Computers and Geotechnics, 33(6-7):316-329.

[13] Bernaud D.; Deudé V.; Dormieux L.; Maghous S.; Schmitt D.P., 2002, *Evolution of elastic properties in finite poroplasticity and finite element analysis*, International Journal for Numerical and Analytical Methods in Geomechanics, 26(9):845-871.

[14] Hashin Z., 1983, *Analysis of composite materials - a survey*, Journal of Applied Mechanics, 50(3):481-505.

[15] Wood D.M., 1990, *Soil Behaviour and critical state soil mechanics*, Cambridge University Press.

[16] Barthelemy, J.F.; Dormieux, L.; Maghous, S., 2003, *Micromechanical approach to the modelling of compaction at large strains*, Computers and Geotechnics, 30:321-338.

[17] Deudé V.; Dormieux L.; Maghous S.; Barthélémy J.F.; Bernaud D., 2004, *Compaction process in sedimentary basins: the role of stiffness increase and hardening induced by large plastic strains*, International Journal for Numerical and Analytical Methods in Geomechanics, 28(13):1279-1303.

[18] Bathe K.J., 1996, *Finite element procedures*, Prentice-Hall, Upper Saddle River.

[19] Hamilton E.L., 1959, *Thickness and consolidation of deep-sea sediments*. Geological Society of America Bulletin, 70(11):1399-1424.